# Brief Papers

## Adaptive Control of an Autonomous Underwater Vehicle: Experimental Results on ODIN

Gianluca Antonelli, Stefano Chiaverini, Nilanjan Sarkar, and Michael West

***Abstract*—This paper presents a six-degrees-of-freedom controller for autonomous underwater vehicles. The control algorithm is adaptive in the dynamic parameters that are poorly known and time-varying in the underwater environment. Moreover, the proposed control law adopts quaternions to represent attitude errors, and thus avoids representation singularities that occur when using instead Euler angles description of the orientation. The adaptive controller has been successfully implemented and experimentally validated on omni-directional intelligent navigator (ODIN), an autonomous underwater vehicle that has been designed and built at the University of Hawaii. The experimental results demonstrate the good performance of the proposed controller within the constraints of the sensory system.**

***Index Terms*—Adaptive control, mobile robots, position control, underwater vehicle control.**

### I. Introduction

In recent years, several advanced control techniques have been developed for autonomous underwater vehicles (AUVs) and remotely operated vehicles (ROVs), aimed at improving the capability of tracking given reference position and attitude trajectories [12].

AUVs performing manipulation or inspection tasks need to be controlled in six degrees of freedom (dofs). Even though the control problem is kinematically similar to the control of a rigid body in a six-dimensional space, which has been largely studied in the literature, the presence of hydrodynamic effects makes the problem of controlling an AUV much more challenging.

In [28], an adaptive control law has been proposed for the control of an AUV based on Euler angles representation of the orientation and simulation results are provided to show the effectiveness of the proposed approach. Experimental results on omni-directional intelligent navigator (ODIN) in 6 dofs are reported in [6] and [17]. It is, however, well known that the use of minimal attitude descriptions, such as Euler angles, is subject to the occurrence of representation singularities; these can be avoided by resorting to quaternions [21].

Reference [23] presents the state of the art of several existing AUVs and their control architecture. Some of these well-known AUVs are *ABE* of the Woods Hole Oceanographic Institution, *OTTER* from the Monterey Bay Acquarium and Stanford University, *Phoenix* belonging to the Naval Postgraduate School, *Twin Burgers* developed at the University of Tokyo, *OEX* from the Florida Atlantic University [11], and *MARIUS* developed at the Instituto Superior Técnico of Lisbon [18]. Reference [9] describes the control architecture of *VORTEX*, a vehicle developed by Inria and Ifremer, and of *OTTER*.

Focusing on the low-level motion control of AUVs, most of the proposed control schemes take into account the uncertainty in the model by resorting to an adaptive strategy [5], [8], [28] or a robust approach [7], [10], [15], [26], [27]. References [19], [20] report some results on fault tolerance control of AUV's including experimental results on ODIN. In [15], an estimation of the dynamic parameters of the vehicle NPS AUV *Phoenix* is also provided. An overview of control techniques for AUV's is reported in [12].

As for the use of quaternions to control AUVs, [13] and [14] propose several quaternion based control laws. However, these control laws require dynamic compensation; in addition, their effectiveness has been demonstrated only in simulation. In [1], a controller that does not need velocity measurements is proposed. As remarked in [24], few papers concern 6 dofs experiments as in, e.g., [3], [17], and [19].

In this paper, following the adaptive approach for underwater vehicle-manipulator systems proposed in [2], a control law is introduced based on a quaternion attitude representation. A Lyapunov-like stability analysis of the adaptive control algorithm is developed, and the resulting control scheme is validated in 6-dofs experiments. Practical aspects of the implementation are also discussed. The experiments reported in this paper have been performed on ODIN, an AUV that has been developed at the Autonomous Systems Laboratory (ASL) of the University of Hawaii, at the University of Hawaii swimming pool; preliminary experimental results on this system are reported in [3]. The obtained experimental results demonstrate the good performance of the proposed controller.

Manuscript received April 19, 2000; revised December 22, 2000. Manuscript received in final form March 5, 2001. Recommended by Associate Editor K. Kozlowski. The autonomous underwater vehicle ODIN used for this study was sponsored in part by the NSF PYI Award (BES91–57896,PI:Yuh), in part by NSF (BES97–01614,PI:Yuh), in part by ONR (N00014–97-1–0961,PI:Yuh).

G. Antonelli and S. Chiaverini are with the Dipartimento di Automazione, Elettromagnetismo, Ingegneria dell'Informazione e Matematica Industriale, Università degli Studi di Cassino, 03043 Cassino (FR), Italy (e-mail: antonelli@unicas.it, chiaverini@unicas.it).

N. Sarkar is with the Department of Mechanical Engineering, Vanderbilt University, Nashville, TN 37235 USA (e-mail: nilanjan.sarkar@vanderbilt.edu).

M. West is with the Autonomous Systems Laboratory, Mechanical Engineering Department, University of Hawaii at Manoa, Honolulu, HI 96822 USA (e-mail: mwest@spectra.eng.hawaii.edu).

Publisher Item Identifier S 1063-6536(01)04944-2.

## II. Modeling

Let us define the vector $\boldsymbol{\eta} = [\boldsymbol{\eta}_1^{\mathrm{T}} \quad \boldsymbol{\eta}_2^{\mathrm{T}}]^{\mathrm{T}}$, where $\boldsymbol{\eta}_1 = [x \quad y \quad z]^{\mathrm{T}} \in \mathbb{R}^3$ is the vector of vehicle position coordinates in a earth-fixed reference frame and $\boldsymbol{\eta}_2 = [\phi \quad \theta \quad \psi]^{\mathrm{T}} \in \mathbb{R}^3$ is the vector of vehicle Euler-angle coordinates in a earth-fixed reference frame, and the vector $\boldsymbol{\nu} = [\boldsymbol{\nu}_1^{\mathrm{T}} \quad \boldsymbol{\nu}_2^{\mathrm{T}}]^{\mathrm{T}}$, where $\boldsymbol{\nu}_1 = [u \quad v \quad w]^{\mathrm{T}} \in \mathbb{R}^3$ is the vector of vehicle linear velocity expressed in the vehicle-fixed reference frame and $\boldsymbol{\nu}_2 = [p \quad q \quad r]^{\mathrm{T}} \in \mathbb{R}^3$ is the vector of vehicle angular velocity expressed in the vehicle-fixed reference frame. In Fig. 1, the defined frames and the elementary vehicle motions are illustrated.

The vehicle-fixed linear and angular velocity $\boldsymbol{\nu}$ and the time derivative of the earth-fixed vehicle position coordinates are related by the following relationships:

$$\boldsymbol{\nu} = \begin{bmatrix} \boldsymbol{R}_I^B(\boldsymbol{\eta}_2) & \boldsymbol{O}_{3\times 3} \\ \boldsymbol{O}_{3\times 3} & \boldsymbol{T}(\boldsymbol{\eta}_2) \end{bmatrix} \dot{\boldsymbol{\eta}} \tag{1}$$

where $\boldsymbol{R}_I^B$ is the rotation matrix expressing the transformation from the inertial frame to the body-fixed frame $\boldsymbol{O}_{n_1\times n_2}$ is the $(n_1 \times n_2)$ null matrix. The transformation matrix $\boldsymbol{T} \in \mathbb{R}^{3\times 3}$ can be expressed in terms of Euler angles as

$$\boldsymbol{T}(\boldsymbol{\eta}_2) = \begin{bmatrix} 1 & 0 & -s_\theta \\ 0 & c_\phi & c_\theta s_\phi \\ 0 & -s_\phi & c_\theta c_\phi \end{bmatrix} \tag{2}$$

where $c_\alpha$ and $s_\alpha$ are short notations for $\cos(\alpha)$ and $\sin(\alpha)$, respectively. The matrix $\boldsymbol{T}(\boldsymbol{\eta}_2)$ is not invertible for every value of $\boldsymbol{\eta}_2$; in fact, it is singular for $\theta = (2m+1)\pi/2$rads, with $m \in \mathbb{N}$, i.e., for a pitch angle of $\pm(\pi/2)$rads [22]. This singularity is defined as a *representation singularity*. Notice that linear velocity does not suffer from representation singularities due to the full rank of the rotation matrix.

The equations of motion of an AUV can be written in the vehicle-fixed reference frame in the form [28]

$$\boldsymbol{M}\dot{\boldsymbol{\nu}} + \boldsymbol{C}(\boldsymbol{\nu})\boldsymbol{\nu} + \boldsymbol{D}(\boldsymbol{\nu})\boldsymbol{\nu} + \boldsymbol{g}(\boldsymbol{\eta}_2) = \boldsymbol{\tau} \tag{3}$$

where

- $\boldsymbol{M} \in \mathbb{R}^{6\times 6}$ mass matrix that includes both rigid body mass and added mass;
- $\boldsymbol{C}(\boldsymbol{\nu})\boldsymbol{\nu} \in \mathbb{R}^6$ vector of Coriolis and Centrifugal terms including the added mass;
- $\boldsymbol{D}(\boldsymbol{\nu})\boldsymbol{\nu} \in \mathbb{R}^6$ vector of friction and hydrodynamic damping terms;
- $\boldsymbol{g}(\boldsymbol{\eta}_2) \in \mathbb{R}^6$ vector of gravitational and buoyant generalized forces;
- $\boldsymbol{\tau} \in \mathbb{R}^6$ vector of forces and moments acting on the vehicle.

Fluidodynamic theory is rather complex and it is difficult to develop a reliable model for most of the hydrodynamic effects. A rigorous analysis for incompressible fluids would require the implementation of the Navier–Stokes equations (distributed fluid-flow). However, in this work, modeling of the hydrodynamic effects in the context of automatic control is considered. Generally, we are interested in a physical phenomenon only if it significantly affects the dynamic properties of the system under consideration.

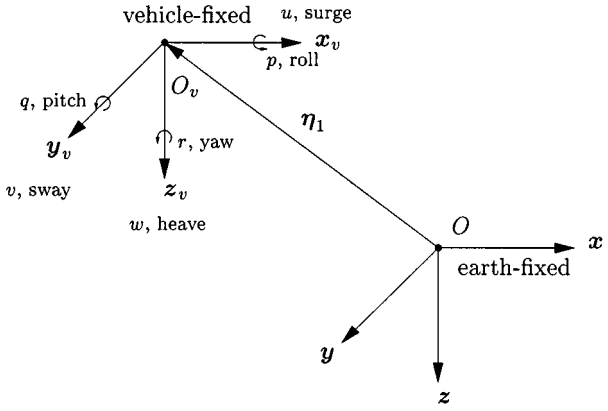


Fig. 1. Frames and elementary motions of the vehicle.

It can be proven that [12]:

- the inertia matrix (including the added mass) is symmetric and positive definite, i.e., $\boldsymbol{M} = \boldsymbol{M}^{\mathrm{T}} > \boldsymbol{O}$;
- the matrix $\boldsymbol{C}(\boldsymbol{\nu})$ (including the added mass) is skew-symmetric.

The viscosity of the fluid also causes the presence of dissipative drag and lift forces on the body. A common simplification is to consider only linear and quadratic damping term and group these terms in a matrix $\boldsymbol{D}$ such that

$$\boldsymbol{D}(\boldsymbol{\nu}) > \boldsymbol{O} \quad \forall\, \boldsymbol{\nu} \in \mathbb{R}^6. \tag{4}$$

The coefficients of this matrix are also considered to be constant. Viscous effects can be considered as the sum of two forces, the *drag* and the *lift* forces. The former is parallel to the relative velocity between the body and the fluid, while the latter is normal to it. Both drag and lift forces are supposed to act at the center of mass of the body. In order to solve the distributed flow problem, an integral over the entire surface is required to compute the net force/moment acting on the body. Moreover, the model of drag and lift forces is not known and, also for some widely accepted models, the coefficients are not known and time-varying.

The relationship between the force/moment acting on the vehicle $\boldsymbol{\tau} \in \mathbb{R}^6$ and the control input of the thrusters $\boldsymbol{u} \in \mathbb{R}^l$ is highly nonlinear. A detailed theoretical and experimental analysis of thrusters' behavior can be found in [16], [25]. Generally, thrusters are the main cause of limit cycle in vehicle positioning and bandwidth constraint. A simplified relationship can be expressed through the linear mapping [12]

$$\boldsymbol{\tau} = \boldsymbol{B}\boldsymbol{u} \tag{5}$$

where $\boldsymbol{B} \in \mathbb{R}^{6\times l}$ is known and constant being $l$ the number of control inputs, e.g., the number of thrusters. In the remainder, we will assume $l \geq 6$ and $\boldsymbol{B}$ being full-rank.

On the other hand, if the vehicle is controlled by thrusters, each of which is locally fed back by the use of a torque sensor, the effects of the nonlinearities discussed above is very limited and a linear input–output relation between desired force/moment and thrusters' inputs is experienced. This is the case, e.g.,

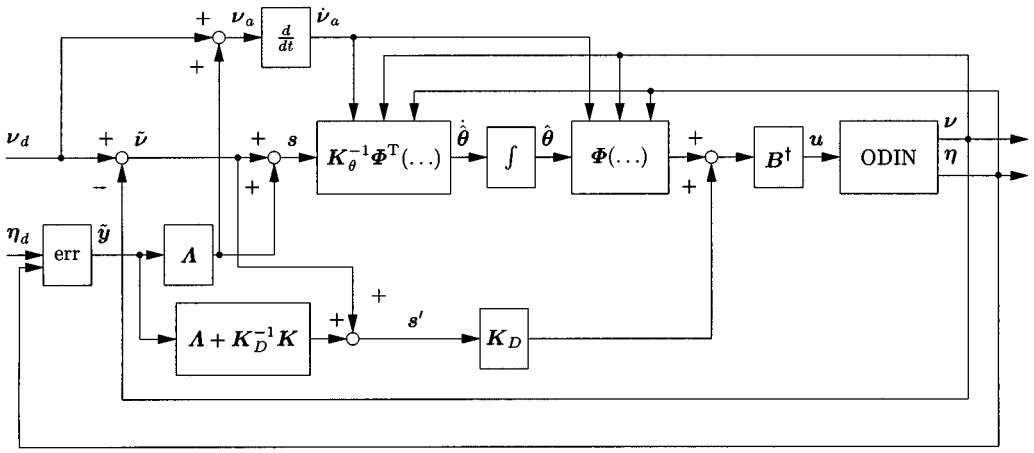


Fig. 2. Block diagram of the control law, the block "err" represents the computation of the position/orientation errors as shown in (10).

of ODIN [3], [5], [17] where the experimental results show that the linear approximation is reliable.

It must be noted that the vehicle attitude dependence is present in the vehicle-fixed dynamic model given by (3) only through the term $\boldsymbol{g}(\boldsymbol{\eta}_2)$. Therefore, to obtain a dynamic model free of representation singularities it is necessary to replace the Euler-angle description of orientation in $\boldsymbol{\eta}_2$ with a suitable attitude representation, e.g., quaternions. In the following, the symbol $\mathcal{Q}$ will be used to denote attitude dependency expressed by quaternions (see the Appendix).

Equation (3) can be rewritten in a matrix form that exploits the linearity in the parameters

$$\boldsymbol{\Phi}(\mathcal{Q}, \boldsymbol{\nu}, \dot{\boldsymbol{\nu}}) \cdot \boldsymbol{\theta} = \boldsymbol{\tau} \tag{6}$$

where $\boldsymbol{\theta} \in \mathbb{R}^{n_\theta}$ is the vector of the dynamic parameters, and $\boldsymbol{\Phi} \in \mathbb{R}^{6 \times n_\theta}$ is the regressor matrix. Notice that $n_\theta$ depends on the model used for the hydrodynamic generalized forces. An estimate is given in [15], where $n_\theta > 100$. For a rigid body moving on the earth's surface the vector of dynamic parameters is constituted simply by the mass, the inertia matrix and the first moment of inertia. For a rigid body moving in a fluid, the dynamic parameters corresponding to the first moment of buoyancy and the hydrodynamic effects must be taken into account. Notice that the linearity in the parameters has been demonstrated for ground-fixed robotic structures [22]; this can be easily extended in order to include the buoyancy effect. However, proper modeling of the other hydrodynamic effects must be adopted so that all dynamic parameters in the model satisfy this property.

Control of marine vehicles cannot neglect the effects of the ocean current. Let us assume that the current, expressed in the inertial frame, $\boldsymbol{\nu}_c^I$ is constant and irrotational, i.e., $\boldsymbol{\nu}_c^I = [\nu_{c,x} \quad \nu_{c,y} \quad \nu_{c,z} \quad 0 \quad 0 \quad 0]^{\mathrm{T}}$ and $\dot{\boldsymbol{\nu}}_c^I = \boldsymbol{0}$. Its effects can be added to the dynamics of a rigid body moving in a fluid simply considering the *relative* velocity in body-fixed frame

$$\boldsymbol{\nu}_r = \boldsymbol{\nu} - \boldsymbol{R}_I^B \boldsymbol{\nu}_c^I \tag{7}$$

in the derivation of the Coriolis and centrifugal terms and the damping terms.

## III. Proposed Control Law

The proposed control law is

$$\boldsymbol{u} = \boldsymbol{B}^\dagger [\boldsymbol{K}_D \boldsymbol{s}' + \boldsymbol{\Phi}(\mathcal{Q}, \boldsymbol{\nu}, \dot{\boldsymbol{\nu}}_a)\hat{\boldsymbol{\theta}}] \tag{8}$$

$$\dot{\hat{\boldsymbol{\theta}}} = \boldsymbol{K}_\theta^{-1} \boldsymbol{\Phi}^{\mathrm{T}}(\mathcal{Q}, \boldsymbol{\nu}, \dot{\boldsymbol{\nu}}_a)\boldsymbol{s} \tag{9}$$

where $\boldsymbol{B}^\dagger$ is the pseudoinverse of matrix $\boldsymbol{B}$, $\boldsymbol{K}_\theta > \boldsymbol{O}, \boldsymbol{K}_D > \boldsymbol{O}$, and $\boldsymbol{\Phi}$ is the system regressor defined in (6). The vectors $\boldsymbol{s}' \in \mathbb{R}^6$ and $\boldsymbol{s} \in \mathbb{R}^6$ are defined as follows:

$$\begin{aligned} \boldsymbol{s}' &= \begin{bmatrix} \tilde{\boldsymbol{\nu}}_1 \\ \tilde{\boldsymbol{\nu}}_2 \end{bmatrix} + (\boldsymbol{\Lambda} + \boldsymbol{K}_D^{-1}\boldsymbol{K}) \begin{bmatrix} \boldsymbol{R}_I^B \tilde{\boldsymbol{\eta}}_1 \\ \tilde{\boldsymbol{\varepsilon}} \end{bmatrix} \\ &= \tilde{\boldsymbol{\nu}} + (\boldsymbol{\Lambda} + \boldsymbol{K}_D^{-1}\boldsymbol{K})\, \tilde{\boldsymbol{y}} \end{aligned} \tag{10}$$

$$\boldsymbol{s} = \tilde{\boldsymbol{\nu}} + \boldsymbol{\Lambda}\tilde{\boldsymbol{y}} \tag{11}$$

with $\tilde{\boldsymbol{\eta}}_1 = \boldsymbol{\eta}_{d,1} - \boldsymbol{\eta}_1$, $\tilde{\boldsymbol{\nu}} = \boldsymbol{\nu}_d - \boldsymbol{\nu}$, where the subscript $d$ denotes desired values for the relevant variables. The vector $\tilde{\boldsymbol{\varepsilon}} \in \mathbb{R}^3$ is the attitude error expressed by quaternions; details on quaternions are given in the Appendix. $\boldsymbol{\Lambda}$ is defined as $\boldsymbol{\Lambda} = \text{blockdiag}\{\lambda_p \boldsymbol{I}_{3\times3}, \lambda_o \boldsymbol{I}_{3\times3}\}$, where $\boldsymbol{I}_{3\times3}$ is the $(3 \times 3)$ identity matrix, $\boldsymbol{\Lambda} > \boldsymbol{O}$. $\boldsymbol{K}$ is defined as $\boldsymbol{K} = \text{blockdiag}\{k_p \boldsymbol{I}_{3\times3}, k_o \boldsymbol{I}_{3\times3}\}$, $\boldsymbol{K} > \boldsymbol{O}$. Finally, it is $\boldsymbol{\nu}_a = \boldsymbol{\nu}_d + \boldsymbol{\Lambda}\tilde{\boldsymbol{y}}$.

A block diagram of the control law is presented in Fig. 2.

### A. Characteristics of the Control Law

The control law is based on a proportional derivative (PD) action with an adaptive compensation of the dynamics aimed at guaranteeing null steady-state error in the presence of constant external disturbances and partial knowledge of the dynamics. It is well known, in fact, that adaptive actions give advantage with respect to simple integral actions on the error variables [4].

The proposed control law is not significantly different from classic adaptive controllers e.g., those for position/orientation control of rigid bodies. Nevertheless the effectiveness of the controllers is seldom verified in full degrees of freedom experiments [24], as done instead in this paper. To achieve an effective implementation, a simple expression for the regressor has been derived in Section IV-B which takes into account only terms which would cause steady-state tracking errors.

Notice that the desired attitude trajectory can be given in terms of roll, pitch and yaw Euler angles despite the fact that the control law makes use of quaternions. The transformation from Euler angles to quaternions, in fact, is free from representation singularities. This is also true for the attitude sensor readings that, in marine environment, are often given by inertial systems in terms of roll, pitch, and yaw angles as well.

### *B. Stability Analysis*

In this section, we will show that the proposed control law (8)–(11) is stable in a Lyapunov-like sense. Let us define the following partition for the variable $\boldsymbol{s}$ that will be useful later:

$$\boldsymbol{s} = \begin{bmatrix} \boldsymbol{s}_p \\ \boldsymbol{s}_o \end{bmatrix} \tag{12}$$

with $\boldsymbol{s}_p \in \mathbb{R}^3$ and $\boldsymbol{s}_o \in \mathbb{R}^3$, respectively.

We consider the scalar function $V(\tilde{\boldsymbol{y}}, \boldsymbol{s}, \tilde{\boldsymbol{\theta}})$

$$\begin{aligned} V =& \frac{1}{2}\boldsymbol{s}^{\mathrm{T}}\boldsymbol{M}\boldsymbol{s} + \frac{1}{2}\tilde{\boldsymbol{\theta}}^{\mathrm{T}}\boldsymbol{K}_\theta\tilde{\boldsymbol{\theta}} + \\ &+ \frac{1}{2}\begin{bmatrix} \tilde{\boldsymbol{\eta}}_1 \\ \tilde{\boldsymbol{z}} \end{bmatrix}^{\mathrm{T}} \begin{bmatrix} k_p\boldsymbol{I}_{3\times 3} & \boldsymbol{O}_{3\times 4} \\ \boldsymbol{O}_{4\times 3} & 2k_o\boldsymbol{I}_{4\times 4} \end{bmatrix} \begin{bmatrix} \tilde{\boldsymbol{\eta}}_1 \\ \tilde{\boldsymbol{z}} \end{bmatrix} \end{aligned} \tag{13}$$

where $\tilde{\boldsymbol{z}} = [1 \quad \boldsymbol{0}^{\mathrm{T}}]^{\mathrm{T}} - \boldsymbol{z} = [1 - \tilde{\eta} \quad -\tilde{\boldsymbol{\varepsilon}}^{\mathrm{T}}]^{\mathrm{T}}$. $V > 0$ in view of positive definiteness of $\boldsymbol{M}$, $\boldsymbol{K}_\theta$, $k_p$, and $k_o$. The scalar function $V$ is then lower bounded.

Differentiating $V$ with respect to time yields

$$\dot{V} = \boldsymbol{s}^{\mathrm{T}}\boldsymbol{M}\dot{\boldsymbol{s}} + \tilde{\boldsymbol{\theta}}^{\mathrm{T}}\boldsymbol{K}_\theta\dot{\tilde{\boldsymbol{\theta}}} + k_p\tilde{\boldsymbol{\eta}}_1^{\mathrm{T}}\boldsymbol{R}_B^I\tilde{\boldsymbol{\nu}}_1 - 2k_o\tilde{\boldsymbol{z}}^{\mathrm{T}}\boldsymbol{U}(\boldsymbol{z})\tilde{\boldsymbol{\nu}}_2 \tag{14}$$

where $\boldsymbol{U}(\boldsymbol{z})$ is defined in the Appendix. Observing that, in view of (11) and (12) it is

$$\tilde{\boldsymbol{\nu}}_1 = \boldsymbol{s}_p - \lambda_p\boldsymbol{R}_I^B\tilde{\boldsymbol{\eta}}_1 \tag{15}$$

$$\tilde{\boldsymbol{\nu}}_2 = \boldsymbol{s}_o - \lambda_o\tilde{\boldsymbol{\varepsilon}} \tag{16}$$

and taking into account (3), (15), and (16), (14) can be rewritten as

$$\begin{aligned} \dot{V} =& \boldsymbol{s}^{\mathrm{T}}[\boldsymbol{M}\dot{\boldsymbol{\nu}}_a - \boldsymbol{B}\boldsymbol{u} + \boldsymbol{C}(\boldsymbol{\nu})\boldsymbol{\nu} + \boldsymbol{D}(\boldsymbol{\nu})\boldsymbol{\nu} + \boldsymbol{g}] \\ &- \tilde{\boldsymbol{\theta}}^{\mathrm{T}}\boldsymbol{K}_\theta\dot{\tilde{\boldsymbol{\theta}}} + k_p\tilde{\boldsymbol{\eta}}_1^{\mathrm{T}}\boldsymbol{R}_B^I\boldsymbol{s}_p - k_p\lambda_p\tilde{\boldsymbol{\eta}}_1^{\mathrm{T}}\tilde{\boldsymbol{\eta}}_1 \\ &+ k_o\tilde{\boldsymbol{\varepsilon}}^{\mathrm{T}}\boldsymbol{s}_o - \lambda_o k_o\tilde{\boldsymbol{\varepsilon}}^{\mathrm{T}}\tilde{\boldsymbol{\varepsilon}} \end{aligned} \tag{17}$$

where we have assumed $\dot{\tilde{\boldsymbol{\theta}}} = -\dot{\hat{\boldsymbol{\theta}}}$, i.e., the dynamic parameters are constant.

Exploiting (6), (17) can be rewritten in compact form

$$\begin{aligned} \dot{V} =& \boldsymbol{s}^{\mathrm{T}}[\boldsymbol{\Phi}(\mathcal{Q}, \boldsymbol{\nu}, \dot{\boldsymbol{\nu}}_a)\boldsymbol{\theta} - \boldsymbol{B}\boldsymbol{u} + \boldsymbol{K}\tilde{\boldsymbol{y}}] - \tilde{\boldsymbol{\theta}}^{\mathrm{T}}\boldsymbol{K}_\theta\dot{\tilde{\boldsymbol{\theta}}} \\ &- \begin{bmatrix} \tilde{\boldsymbol{\eta}}_1 \\ \tilde{\boldsymbol{\varepsilon}} \end{bmatrix}^{\mathrm{T}} \begin{bmatrix} k_p\lambda_p\boldsymbol{I}_{3\times 3} & \boldsymbol{O}_{3\times 3} \\ \boldsymbol{O}_{3\times 3} & k_o\lambda_o\boldsymbol{I}_{3\times 3} \end{bmatrix} \begin{bmatrix} \tilde{\boldsymbol{\eta}}_1 \\ \tilde{\boldsymbol{\varepsilon}} \end{bmatrix}. \end{aligned} \tag{18}$$

Plugging the control law (8)–(11) into (18) and taking into account the definition of $\tilde{\boldsymbol{y}}$, we finally obtain

$$\dot{V} = -\boldsymbol{s}^{\mathrm{T}}\boldsymbol{K}_D\boldsymbol{s} - \tilde{\boldsymbol{y}}^{\mathrm{T}} \begin{bmatrix} \boldsymbol{R}_I^B k_p\lambda_p\boldsymbol{R}_B^I & \boldsymbol{O}_{3\times 3} \\ \boldsymbol{O}_{3\times 3} & k_o\lambda_o\boldsymbol{I}_{3\times 3} \end{bmatrix} \tilde{\boldsymbol{y}} \tag{19}$$

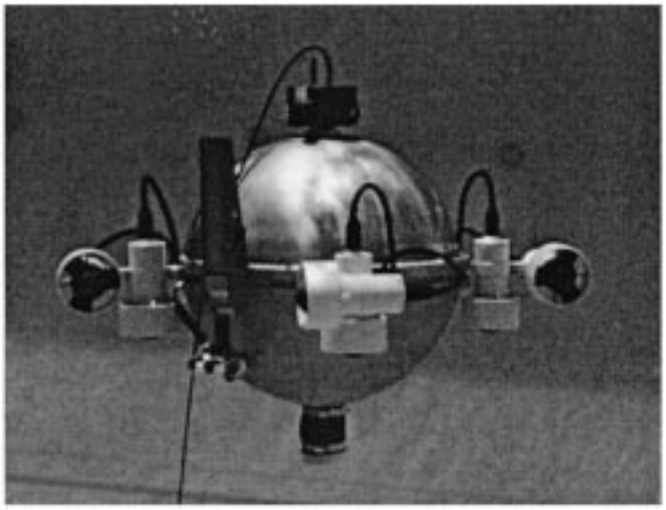

Fig. 3. Picture of ODIN, an AUV that has been designed and built at the University of Hawaii.

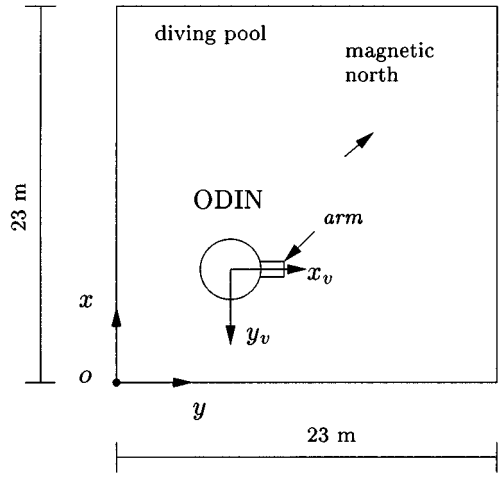


Fig. 4. Sketch of the pool with relevant frames.

that is negative semidefinite over the state space $\{\tilde{\boldsymbol{y}}, \boldsymbol{s}, \tilde{\boldsymbol{\theta}}\}$.

We can now prove the system stability in a Lyapunov-like sense using the Barbalat's lemma. The following conditions hold:

- $V$ is lower bounded;
- $\dot{V}(\tilde{\boldsymbol{y}}, \boldsymbol{s}, \tilde{\boldsymbol{\theta}}) \leq 0$;
- $\dot{V}(\tilde{\boldsymbol{y}}, \boldsymbol{s}, \tilde{\boldsymbol{\theta}})$ is uniformly continuous;

then $\dot{V}(\tilde{\boldsymbol{y}}, \boldsymbol{s}, \tilde{\boldsymbol{\theta}}) \to 0$ as $t \to \infty$.

Thus $\tilde{\boldsymbol{y}}, \boldsymbol{s} \to \boldsymbol{0}$ as $t \to \infty$ ($\tilde{\boldsymbol{\theta}}$ does not appear explicitly in $\dot{V}$). In view of (11) and the decreasing behavior of $\tilde{\boldsymbol{y}}$, also $\tilde{\boldsymbol{\nu}} \to \boldsymbol{0}$ as $t \to \infty$. Moreover, due to the full rank of the rotation matrix $\boldsymbol{R}_I^B$, also $\tilde{\boldsymbol{\varepsilon}}, \tilde{\boldsymbol{\eta}}_1 \to \boldsymbol{0}$ as $t \to \infty$. We can thus conclude that the position and orientation errors in the earth-fixed frame are null at steady-state with a bounded $\tilde{\boldsymbol{\theta}}$. This means that the estimate $\hat{\boldsymbol{\theta}}$ may not converge to the true value of the dynamic parameters; however, this does not affect asymptotic tracking of the position and orientation trajectory.

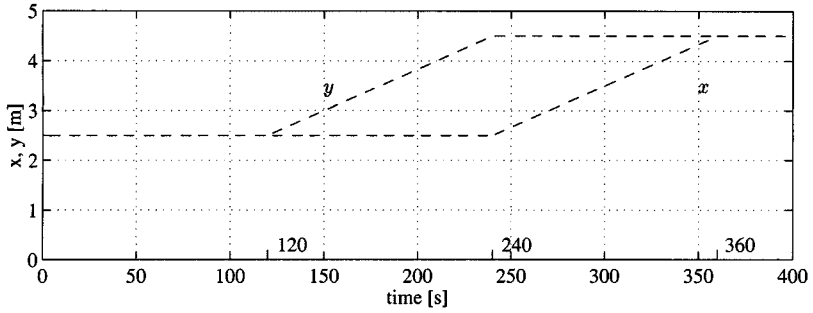


Fig. 5. Time history of the vehicle's desired $x$ and $y$ position.

## IV. Experimental Results

### A. Experimental Setup

ODIN is an autonomous underwater vehicle developed at the ASL of the University of Hawaii. A picture of the vehicle is shown in Fig. 3; it has a near-spherical shape with horizontal diameter of 0.63 m and vertical diameter of 0.61 m, made of anodizied aluminum (AL 6061-T6). Its dry weight is about 125 kg, resulting in a slightly positively buoyant behavior. The processor is a Motorola 68040/33 MHz working with VxWorks 52 operating system. The power supply is provided by 24 Lead Gel batteries; 20 batteries are used for the thrusters and four for the CPU. It provides about two hours of autonomous operation. The actuating system is made of eight marine propellers built at ASL, which are actuated by brushless motors. Each motor weighs about 1 kg and can provide a maximum thrust force of about 27 N. The sensory system is composed of: a pressure sensor for depth measurement, with an accuracy of 3 cm; eight sonars for position reconstruction and navigation, each with a range $0.1 : 14.4$ m; an inertial system for attitude and velocity measurements.

### B. Implementation Issues

Despite the closed environment in which the experiments have been conducted, the swimming pool of the University of Hawaii, it is necessary to take into account the presence of a current as an irrotational, constant disturbance [12]. In this case, indeed, there exists a current which is sustained by the pump that circulates water in the pool; this current is strong enough to affect the vehicle dynamics.

Since the measure of the current is not available to ODIN, we have taken into account the current as a constant disturbance $\boldsymbol{d}_c$ acting at the force/moment level on the vehicle according to the equation

$$\boldsymbol{M}\dot{\boldsymbol{\nu}} + \boldsymbol{C}(\boldsymbol{\nu})\boldsymbol{\nu} + \boldsymbol{D}(\boldsymbol{\nu})\boldsymbol{\nu} + \boldsymbol{g}(\boldsymbol{\eta}_2) + \boldsymbol{d}_c = \boldsymbol{\tau}. \tag{20}$$

Moreover, since the number of dynamic parameters is very large ($n_\theta > 100$, see [12]) we have implemented a reduced version of the regressor matrix in order to adapt only with respect to the restoring force/moments and to the current. The implemented regressor, for the restoring force part, has then the expression

$$\boldsymbol{\Phi}(\mathcal{Q}) = \begin{bmatrix} \boldsymbol{R}_I^B \boldsymbol{g}^I & \boldsymbol{O}_{3\times 3} \\ \boldsymbol{0}_{3\times 1} & \boldsymbol{S}\left(\boldsymbol{R}_I^B \boldsymbol{g}^I\right) \end{bmatrix} \tag{21}$$

where $\boldsymbol{g}^I = [0 \quad 0 \quad 9.81]^{\mathrm{T}}$ m/s$^2$ $\in \mathbb{R}^3$ is the gravity vector expressed in the earth-fixed frame. The vector of dynamic parameters is then composed by the scalar mass/buoyancy and the $(3 \times 1)$ vector of the center of gravity/buoyancy. It should be noted that we decide not to compensate for the velocity terms, since, for this specific experimental setup, those measures are much noisy.

The use of the pseudoinverse $\boldsymbol{B}^{\dagger}$ in (8) is aimed at locally reducing the norm of the thrusters. If different thrusters, with different energy comsumption, are used, a weighted pseudoinverse could be used. Since ODIN is equipped with eight thrusters of the same type the weight factor is not necessary.

### C. Experiments

The proposed controller has been implemented on ODIN to test its performance. The vehicle is asked to track the following desired trajectory with a trapezoidal velocity profile. Since the sonars need to be under the surface of the water to work properly, the first movement is of 2 m in the $z$ direction (see Fig. 4 for the relevant frames, subscript $v$ stands for vehicle-fixed frame). The vehicle is then asked to move 2 m in the $y$ direction and 2 m in the $x$ direction. The desired path is shown in Figs. 5 and 6. The desired trajectory is quite *simple*, in fact, due to the small dimension of the pool, it was not advisable to command vehicles rotation in order to avoid reflections of the sonar beams into the pool's corners. In that case the sonar readings would be useless. The use of different sensors as, e.g., acoustic baseline, would eliminate such limitation.

The control law has been designed using quaternions, however the specifications of the desired trajectory and the output results are given in Euler angles because of their immediate comprehension. Notice that the transformation from Euler angles to quaternions is free from representation singularities. The attitude is kept constant at the value of $\boldsymbol{\eta}_{d,2} = [0 \quad 0 \quad 90]^{\mathrm{T}}$ deg. Since the vehicle is not perfectly balanced, at rest, i.e., with the thrusters off, its position is $\phi \approx 5^\circ$ and $\theta \approx 15^\circ$ with the yaw depending on the current. The desired orientation, thus, is a set-point for the control task. Moreover, different experiments would lead to different rest positions. This is due to the fact that the centers of gravity and buoyancy are very close and small desplacements of the internal components would results in different equilibrium attitudes. With this in mind, it is obvious that dynamic compensation of such systems is very hard.

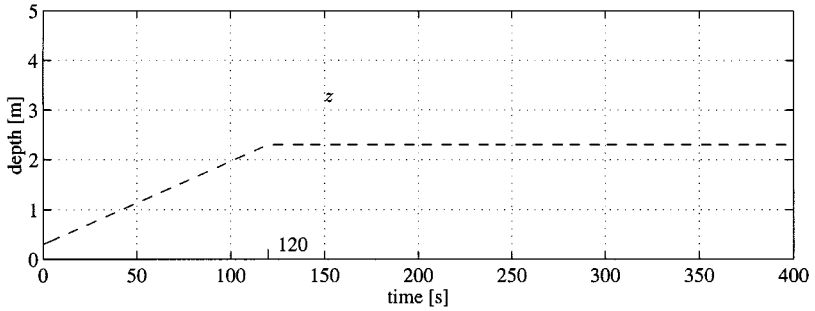


Fig. 6. Time history of the vehicle's desired depth.

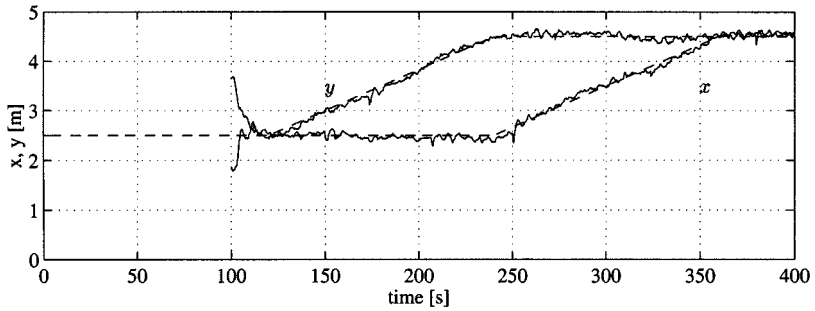


Fig. 7. Experimental results. First experiment: time history of the vehicle $x$ and $y$ position. During the first 100 s the horizontal data are not available and the vehicle is not controlled along those directions.

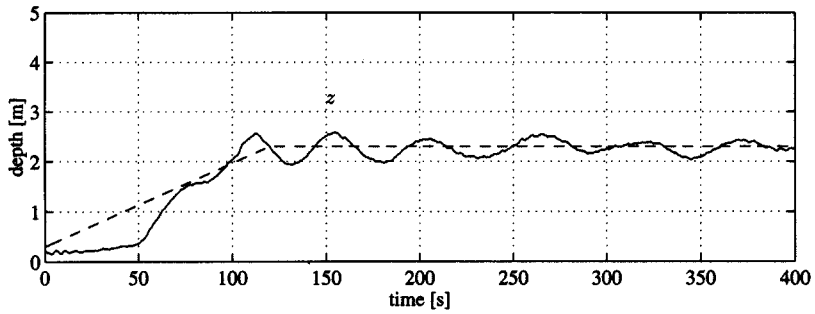


Fig. 8. Experimental results. First experiment: time history of the vehicle depth. Note that the vehicle oscillates in this direction.

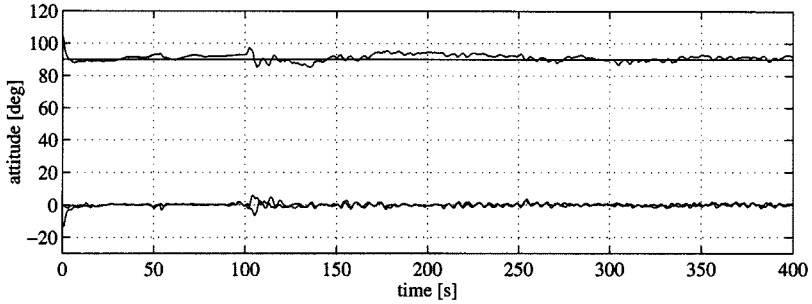


Fig. 9. Experimental results. First experiment: time history of the vehicle's attitude in terms of Euler angles.

Two experiments are presented in this paper. The sampling frequency of the closed loop is 5 Hz. The control gains have been tuned first by simulation and then by trial and error during the experiments. For the first experiment, the following control gains have been used

$$\boldsymbol{\Lambda} = \text{diag}\{0.5 \quad 0.5 \quad 0.1 \quad 0.8 \quad 0.8 \quad 0.8\}$$
$$\boldsymbol{K}_D = \text{diag}\{12 \quad 12 \quad 4 \quad 2 \quad 2 \quad 8\}$$
$$\boldsymbol{K}_\theta = \text{diag}\{0.01 \quad 0.3 \cdot \boldsymbol{I}_{3\times 3}\}.$$

In Figs. 7 and 8, the time history of the position of the vehicle in the inertial frame is shown. Notice that, due to technical characteristics of the horizontal sonars [17], the $x$ and $y$ position data for the first 100 s where not available. The vehicle is not controlled in those directions and subjected to the pool's current. At $t = 100$ s, $\boldsymbol{\eta}_1 = [1.87 \quad 3.66 \quad 2.03]^{\mathrm{T}}$ m and

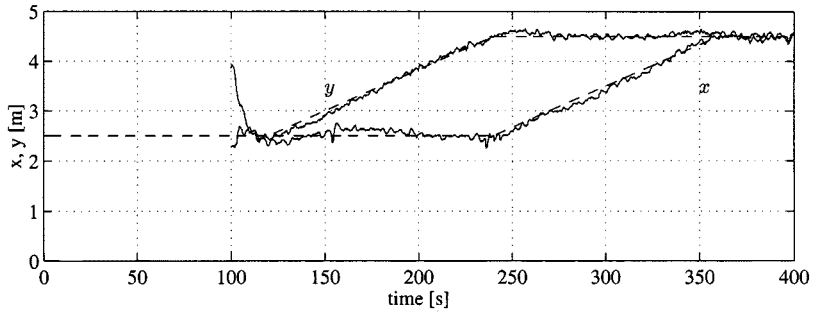


Fig. 10. Experimental results. Second experiment: time history of the vehicle $x$ and $y$ position. During the first 100 s the horizontal data are not available and the vehicle is not controlled on those directions.

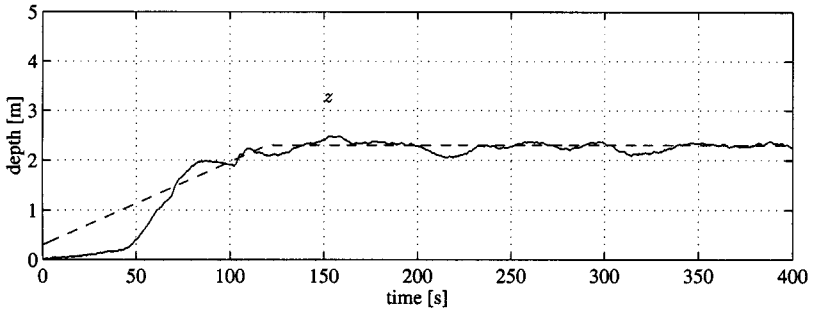


Fig. 11. Experimental results. Second experiment: time history of the vehicle depth. The oscillating behavior of the first experiment is reduced by increasing the damping factor.

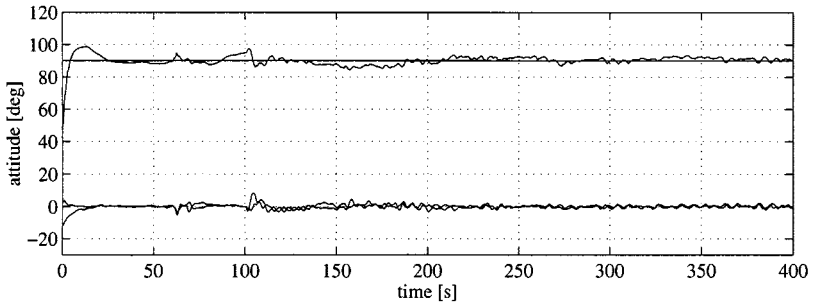


Fig. 12. Experimental results. Second experiment: time history of the vehicle's attitude in terms of Euler angles.

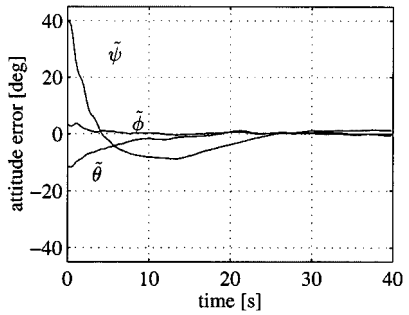


Fig. 13. Experimental results. Second experiment: time history of the vehicle's attitude errors in terms of Euler angles (first 40 s).

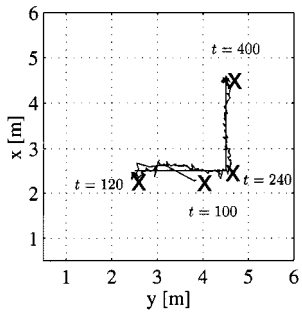


Fig. 14. Experimental results. Second experiment: path on $xy$. At $t = 100$ s the vehicle has to recover the effect of the current.

$\tilde{\boldsymbol{\eta}}_1 = [0.63 \quad -1.16 \quad -0.03]^{\mathrm{T}}$ m, it recovers the desired position and starts tracking the trajectory. At the very beginning of the task execution, the vehicle does not track the desired depth. This is because of the fact that we have assumed that all the dynamic parameters are unknown. As a result, the adaptation action requires time to take effect. From these plots, it is also possible to appreciate the different noise characteristics of the two position sensors, the sonar for the horizontal plane and the pressure sensor for the depth. It is obvious form the $z$ direction trajectory that the system does not have enough damping. The behavior is, however, satisfactory in $x$ and $y$ directions; it is also satisfactory in $\boldsymbol{\eta}_2$, as can be seen in Fig. 9.

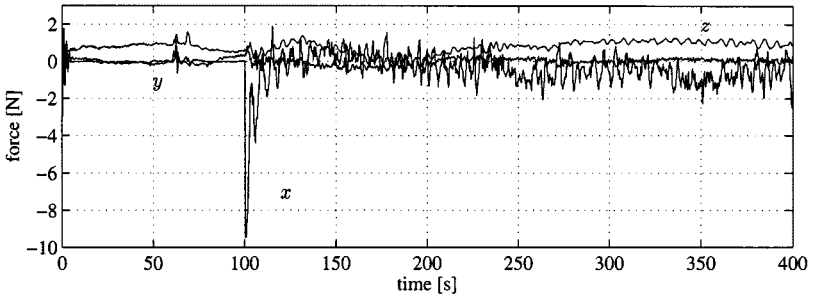


Fig. 15. Experimental results. Second experiment: control forces.

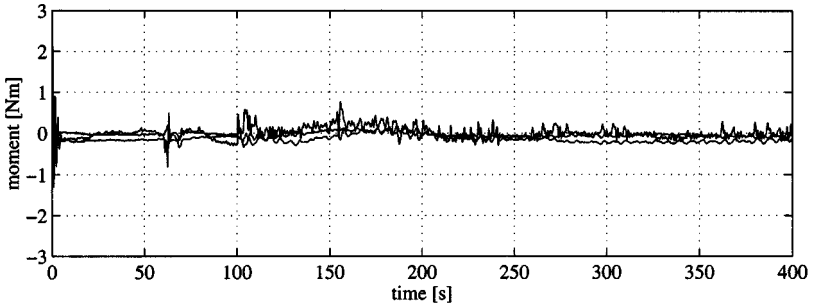


Fig. 16. Experimental results. Second experiment: control moments.

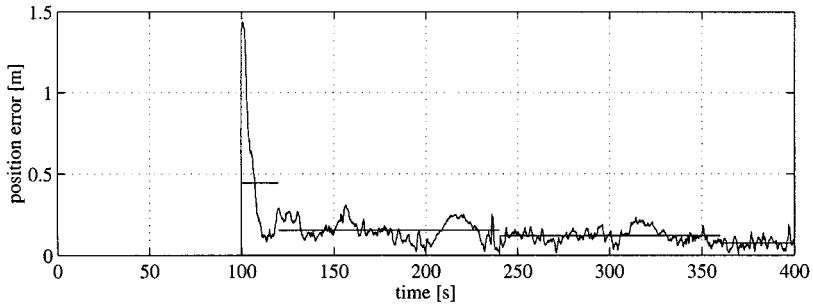


Fig. 17. Experimental results. Second experiment: 2-norm of the linear position error in the inertial frame. The horizontal segments represent the mean values of the error in the corresponding time intervals.

To improve the dynamic response of the system in the $z$ direction, the control gains are modified as follows:

$$\begin{aligned}\boldsymbol{\Lambda} &= \text{diag}\{0.5 \quad 0.5 \quad 0.15 \quad 0.8 \quad 0.8 \quad 0.8\},\\ \boldsymbol{K}_D &= \text{diag}\{12 \quad 12 \quad 5 \quad 2 \quad 2 \quad 8\},\\ \boldsymbol{K}_\theta &= \text{diag}\{0.01 \quad 0.3 \cdot \boldsymbol{I}_{3\times 3}\}\end{aligned}$$

and a second experiment has been conducted.

Notice that, despite the fact that the vehicle is almost spherical, the $z$ control gains are different from $x$ and $y$. In that direction, in fact, when roll and pitch are null, the action of gravity and buoyancy result in a different dynamic behavior as compared to the other directions.

In Figs. 10 and 11, the time history of the position of the vehicle in the inertial frame is shown. Also in this case, at $t = 100$ s, with $\boldsymbol{\eta}_1 = [2.28 \quad 3.87 \quad 1.91]^{\mathrm{T}}$ m, $\tilde{\boldsymbol{\eta}}_1 = [0.22 \quad -1.37 \quad 0.09]^{\mathrm{T}}$ m, the vehicle recovers the desired position and starts tracking successfully the desired trajectory. The depth is now tracked with a more damped behavior.

In Figs. 12 and 13, the attitude of the vehicle and the orientation error in terms of the Euler angles are shown. It can be noticed that the desired attitude is tracked for the overall duration of the experiment and that a small coupling can be seen when, at $t = 100$ s, the horizontal sensory system is started and the vehicle recovers the desired position in the plane. In detail, in Fig. 13, a zoom of the first 40 s is shown.

In Fig. 14, the path in the horizontal plane is shown. It can be noted that the second segment is followed with a smaller error than the first, due to the adaptation action. Also, the position at $t = 100$ s, $x = 2.28$ m, $y = 3.87$ m, is due to the effect of the current.

In Figs. 15 and 16, the control actions are shown. The *peak* in $\boldsymbol{\tau}_x$ is due to the large error *seen* by the controller at $t = 100$ s. Also note the presence of noise in the sensor readings as evident from the position plots.

Finally, in Fig. 17, the 2-norm of the position error ($x$, $y$, and $z$ components) is shown. The lines represent the mean values of the corresponding time intervals. It can be noted that the mean error at steady state, in the last 40 s, is about 7 cm. This value must be related to the low accuracy (about 2 cm) and the

high noise that affect the sonar's data concerning the $x$ and $y$ earth-fixed coordinates. The position estimation has been partially improved by the use of a Kalman filter [17]. However, the occurrence of several missing readings affected this specific set of experiments thus reducing the performance of the overall closed-loop system.

## V. Conclusion

A 6–DOF adaptive control law has been experimentally validated on ODIN, an AUV. The control law is adaptive in the dynamic parameters that are poorly known in the underwater environment. Moreover, the proposed control law adopts quaternions to represent attitude errors and thus avoids representation singularities that occur when using Euler angle description of orientation. The experimental results are satisfactory within the constraints of the sonar sensory system.

## Appendix
## Attitude Error Representation

By defining the mutual orientation between two frames of common origin in terms of the rotation matrix

$$\boldsymbol{R}_{\boldsymbol{k}}(\delta) = \cos\delta \boldsymbol{I}_{3\times 3} + (1-\cos\delta)\boldsymbol{k}\boldsymbol{k}^{\mathrm{T}} - \sin\delta \boldsymbol{S}(\boldsymbol{k}) \tag{22}$$

where

- $\delta$ angle;
- $\boldsymbol{k} \in \mathbb{R}^3$ unit vector of the axis expressing the rotation needed to align the two frames;
- $\boldsymbol{I}_{3\times 3}$ $(3\times 3)$ identity matrix;
- $\boldsymbol{S}(\cdot)$ matrix operator performing the cross product between two $(3\times 1)$ vectors;

we define the unit quaternion as

$$\mathcal{Q} = \{\eta, \boldsymbol{\varepsilon}\} \quad \eta = \cos\frac{\delta}{2} \quad \boldsymbol{\varepsilon} = \sin\frac{\delta}{2}\boldsymbol{k} \tag{23}$$

where $\eta \geq 0$ for $\delta \in [-\pi, \pi]$. This restriction is necessary for uniqueness of the quaternion associated to a given matrix, in that the two quaternions $\{\eta, \boldsymbol{\varepsilon}\}$ and $\{-\eta, -\boldsymbol{\varepsilon}\}$ represent the same orientation, i.e., the same rotation matrix. The unit quaternion satisfies the condition $\eta^2 + \boldsymbol{\varepsilon}^{\mathrm{T}}\boldsymbol{\varepsilon} = 1$.

The $(3\times 3)$ rotation matrix from the vehicle-fixed frame to the earth-fixed frame, $\boldsymbol{R}_B^I$, is also described by the quaternion $\mathcal{Q}$. Let us also define $\boldsymbol{R}_d^I$ the $(3\times 3)$ rotation matrix from the frame expressing the desired vehicle orientation to the earth-fixed frame, which is also described by the quaternion $\mathcal{Q}_d = \{\eta_d, \boldsymbol{\varepsilon}_d\}$. One possible choice for the rotation matrix necessary to align the two frames is

$$\widetilde{\boldsymbol{R}} = \boldsymbol{R}_I^B \cdot \boldsymbol{R}_d^I \tag{24}$$

where $\boldsymbol{R}_I^B = \boldsymbol{R}_B^{I\,\mathrm{T}}$. The quaternion $\widetilde{\mathcal{Q}} = \{\tilde{\eta}, \tilde{\boldsymbol{\varepsilon}}\}$ associated with $\widetilde{\boldsymbol{R}}$ is easily obtained by

$$\begin{aligned} \tilde{\eta} &= \eta\eta_d + \boldsymbol{\varepsilon}^{\mathrm{T}}\boldsymbol{\varepsilon}_d \\ \tilde{\boldsymbol{\varepsilon}} &= \eta\boldsymbol{\varepsilon}_d - \eta_d\boldsymbol{\varepsilon} + \boldsymbol{S}(\boldsymbol{\varepsilon}_d)\boldsymbol{\varepsilon}. \end{aligned} \tag{25}$$

Since the quaternion associated with $\widetilde{\boldsymbol{R}} = \boldsymbol{I}_{3\times 3}$, i.e., representing two aligned frames, is $\widetilde{\mathcal{Q}} = \{1, \boldsymbol{0}\}$, the vector $\boldsymbol{\varepsilon}$ can be used as a measure of the misalignment of the frames. Thus, it is sufficient to represent the attitude error as $\tilde{\boldsymbol{\varepsilon}}$.

Finally, it is useful to consider the *quaternion propagation equation*

$$\begin{aligned} \dot{\tilde{\eta}} &= -\frac{1}{2}\tilde{\boldsymbol{\varepsilon}}^{\mathrm{T}}\tilde{\boldsymbol{\nu}}_2 \\ \dot{\tilde{\boldsymbol{\varepsilon}}} &= \frac{1}{2}\tilde{\eta}\tilde{\boldsymbol{\nu}}_2 + \frac{1}{2}\boldsymbol{S}(\tilde{\boldsymbol{\varepsilon}})\tilde{\boldsymbol{\nu}}_2, \end{aligned} \tag{26}$$

where $\tilde{\boldsymbol{\nu}}_2 = \boldsymbol{\nu}_{2,d} - \boldsymbol{\nu}_2$ is the angular velocity error expressed in vehicle-fixed frame. Notice that this expression is analogous to the one established through (2) but does not suffer from representation singularities. Defining $\boldsymbol{z} = [\,\tilde{\eta} \quad \tilde{\boldsymbol{\varepsilon}}^{\mathrm{T}}\,]^{\mathrm{T}}$, (26) can be rewritten in the form

$$\dot{\boldsymbol{z}} = \frac{1}{2}\begin{bmatrix} -\tilde{\boldsymbol{\varepsilon}}^{\mathrm{T}} \\ \tilde{\eta}\boldsymbol{I}_{3\times 3} + \boldsymbol{S}(\tilde{\boldsymbol{\varepsilon}}) \end{bmatrix}\tilde{\nu}_2 = \boldsymbol{U}(\boldsymbol{z})\tilde{\nu}_2. \tag{27}$$

## Acknowledgment

The authors are grateful to Dr. J. Yuh for making ODIN available for this study and to Dr. S. Choi for guiding wet tests. The authors also thank Mr. Z. Yao and Mr. J. Lee for their assistance for wet tests.

## References

[1] G. Antonelli, F. Caccavale, S. Chiaverini, and L. Villani, "An output feedback algorithm for position and attitude tracking control of underwater vehicles," in *Proc. 37th IEEE Conf. Decision Contr.*, Tampa, FL, Dec. 1998, pp. 4567–4572.

[2] G. Antonelli and S. Chiaverini, "Adaptive tracking control of underwater vehicle-manipulator systems," in *Proc. 1998 IEEE Int. Conf. Contr. Applicat.*, Trieste, Italy, Sept. 1998, pp. 1089–1093.

[3] G. Antonelli, S. Chiaverini, N. Sarkar, and M. West, "Adaptive control of an autonomous underwater vehicle. experimental results on ODIN," in *Proc. IEEE Int. Symp. Comput. Intell. Robot. Automat.*, Monterey, CA, Nov. 1999, pp. 64–69.

[4] C. C. de Wit, B. Siciliano, and G. Bastin, Eds., *Theory of Robot Control*. Berlin, D, Germany: Springer-Verlag, 1996.

[5] S. K. Choi and J. Yuh, "Experimental study on a learning control system with bound estimation for underwater robots," in *Autonomous Robots*, J. Yuh, T. Ura, and G. A. Bekey, Eds. Boston, MA: Kluwer, 1996, pp. 187–194.

[6] ——, "Experimental study on a learning control system with bound estimation for underwater robots," in *Proc. 1996 IEEE Int. Conf. Robot. Automat.*, Minneapolis, MN, 1996, pp. 2160–2165.

[7] G. Conte and A. Serrani, "Global robust tracking with disturbance attenuation for unmanned underwater vehicles," in *Proc. 1998 IEEE Int. Conf. Contr. Applicat.*, Trieste, Italy, Sept. 1998, pp. 1094–1098.

[8] M. L. Corradini and G. Orlando, "A discrete adaptive variable-structure controller for MIMO systems, and its application to an underwater ROV," *IEEE Trans. Contr. Syst. Technol.*, vol. 5, pp. 349–359, 1997.

[9] E. Coste-Manière, A. Peuch, M. Perrier, V. Rigaud, H. H. Wang, S. M. Rock, and M. J. Lee, "Joint evaluation of mission programming for underwater robots," in *Proc. 1996 IEEE Int. Conf. Robot. Automat.*, Minneapolis, MI, Apr. 1996, pp. 2492–2497.

[10] R. Cristi, F. A. Pappulias, and A. Healey, "Adaptive sliding mode control of autonomous underwater vehicles in the dive plane," *IEEE J. Oceanic Eng.*, vol. 15, pp. 152–160, 1990.

[11] M. Dhanak, E. An, K. Holappa, and S. Smith, "Using small AUV for oceanographic measurements," *MTS/IEEE Ocenas '99*, vol. 3, pp. 1410–1417, 1999.

[12] T. Fossen, *Guidance and Control of Ocean Vehicles*. Chichester, U.K.: Wiley, 1994.

[13] O.-E. Fjellstad and T. I. Fossen, "Quaternion feedback regulation of underwater vehicles," in *Proc. 1994 IEEE Conf. Contr. Applicat.*, Glasgow, U.K., 1994, pp. 857–862.

[14] ——, "Position and attitude tracking of AUVs: A quaternion feedback approach," *IEEE J.Oceanic Eng.*, vol. 19, pp. 512–518, 1994.
[15] A. J. Healey and D. Lienard, "Multivariable sliding mode control for autonomous diving and steering of unmanned underwater vehicles," *IEEE J. Oceanic Eng.*, vol. 18, pp. 327–339, 1993.
[16] A. J. Healey, S. M. Rock, S. Cody, D. Miles, and J. P. Brown, "Toward an improved understanding of thruster dynamics for underwater vehicles," *IEEE J. Oceanic Eng.*, vol. 20, pp. 354–361, 1995.
[17] J. Nie, J. Yuh, E. Kardash, and T. I. Fossen, "On-board sensor-based adaptive control of small UUVS in very shallow water," in *Proc. IFAC Conf. Contr. Applicat. Marine Syst.*, Fukuoka, J, Oct. 1998, pp. 201–206.
[18] P. Oliveira, A. Pascoal, V. Silva, and C. Silvestre, "Design, development, and testing at sea of the mission control system for the MARIUS autonomous underwater vehicle," *MTS/IEEE Ocenas '96*, vol. 1, pp. 401–406, 1996.
[19] T. K. Podder, G. Antonelli, and N. Sarkar, "Fault tolerant control of an autonomous underwater vehicle under thruster redundancy: Simulations and experiments," in *Proc. 2000 IEEE Int. Conf. Robot. Automat.*, San Francisco, CA, April 2000, pp. 1251–1256.
[20] T. K. Podder and N. Sarkar, "Fault tolerant decomposition of thruster forces of an autonomous underwater vehicle," in *Proc. 1999 IEEE Int. Conf. Robot. Automat.*, Detroit, MI, May 1999, pp. 84–89.
[21] R. E. Roberson and R. Schwertassek, *Dynamics of Multibody Systems*. Berlin, Germany: Springer-Verlag, 1988.
[22] L. Sciavicco and B. Siciliano, *Modeling and Control of Robot Manipulators*. London, U.K.: Springer-Verlag, 2000.
[23] K. P. Valavanis, D. Gracanin, M. Matijasevic, R. Kolluru, and G. A. Demetriou, "Control architecture for autonomous underwater vehicles," *IEEE Contr. Syst.*, pp. 48–64, Dec. 1997.
[24] L. L. Whitcomb, "Underwater robotics: Out of the research laboratory and into the field," in *Proc. 2000 IEEE Int. Conf. Robot. Automat.*, San Francisco, CA, Apr. 2000, pp. 709–716.
[25] D. R. Yoerger, J. G. Cooke, and J.-J. Slotine, "The influence of Thruster dynamics on underwater vehicle behavior and their incorporation into control system design," *IEEE J. Oceanic Eng.*, vol. 15, pp. 167–178, 1990.
[26] D. R. Yoerger and J. J. Slotine, "Robust trajectory control of underwater vehicles," *IEEE J. Oceanic Eng.*, vol. 10, pp. 462–470, 1985.
[27] ——, "Adaptive sliding control of an experimental underwater vehicle," in *Proc. 1991 IEEE Int. Conf. Robot. Automat.*, Sacramento, CA, Apr. 1991, pp. 2746–2751.
[28] J. Yuh, "Modeling and control of underwater arobotic vehicles," *IEEE Trans. Syst., Man. Cybern.*, vol. 20, pp. 1475–1483, 1990.